Sustainable Structures
ISSN: 2789-3111 (Print); ISSN: 2789-312X (Online)
http://www.sustain-dpl.com/journal/sust
DOI: 10.54113/j.sust.2026.000107

ORIGINAL ARTICLE

Structural response of glued-laminated bamboo under compression: an experimental and analytical study

Inayat Ullah Khan[a], Haitao Li[b, c], Mahmud Ashraf[a,*]

[a]School of Engineering, Deakin University, Waurn Ponds, Geelong, VIC 3216 Australia.
[b]Jiangsu Carbon Sequestration Materials and Structural Technology of Bamboo & Wood Research Center, Nanjing Forestry University, Nanjing 210037, China
[c] National-provincial joint engineering research center of biomaterials for MACHINERY PACKAGE, Naning Forestry University, Nanjing 210037, China.
[*]Corresponding Author: Mahmud Ashraf, Email: mahmud.ashraf@deakin.edu.au.

Abstract: Glued-laminated bamboo (GLB) is an engineered bamboo product with significant potential for structural applications due to its dimensional stability, compression resistance, and aesthetics. This study investigates the structural response of 84 GLB compression elements of varying lengths and three cross-sectional dimensions. In addition, 12 specimens were tested under three-point bending to evaluate the elastic modulus for structural design purposes. Stress-strain behavior and failure modes were carefully examined to assess the integrity of GLB cross-sections, and an ANOVA was conducted to identify parameters influencing compression performance. Experimental data were used to derive regression models for ultimate load and compressive strength, accurately capturing the observed behavior. Short elements exhibited four stress-strain regions: elastic, hardening, plastic, and softening, whereas long elements failed by buckling with tensile fracture without noticeable plastic deformation. Based on the experimental curves, the Richard–Abbott and Popovics models were applied to simulate the compressive response, with the Richard–Abbott model showing better agreement. Theoretical analyses using GB 50005, Eurocode 5, and the National Design Specification for timber were applied to predict GLB column resistance, and deviations were critically discussed. This study provides insights into the behavior of small-section, high-slenderness GLB compression elements through experimental and analytical approaches.

Keywords: glued laminated bamboo, axial compression, stress-strain behaviour, slenderness ratio, small cross-section elements

1 Introduction

Polymer matrix composites reinforced with glass, aramid, graphite, and carbon fibres are widely used in engineering applications; however, their production consumes significant amounts of energy [1–3]. With increasing resource demand and declining availability in today's industrialized world, it is essential to explore sustainable alternatives for building materials. Bamboo and wood have gained considerable attention in green building communities due to their environmentally friendly characteristics. They are renewable, biodegradable, capable of sequestering atmospheric carbon, and have lower embodied energy and pollution levels during production when compared to steel or concrete

Received: 29 August 2025; Received in revised form: 19 May 2026; Accepted: 28 May 2026

[4]. Notably, structural bamboo can be harvested within 3–4 years, whereas wood requires more than 25 years to harvest [5–7].

Natural bamboo, however, is hollow and non-uniform in geometry, which limits its direct structural use. To overcome this, engineered bamboo products such as glued laminated engineered bamboo (GLB or Glubam) and bamboo scrimber have been developed. Bamboo scrimber is manufactured by compressing bamboo fibre bundles or sheets, whereas GLB is produced by adhesively bonding parallel bamboo strips. Compared to scrimber, GLB requires less adhesive and makes use of bamboo strips in their natural form [8] offering a more sustainable option for wider applications. The current study investigates smaller GLB cross-sections with varying slenderness ratios that have the potential for use in bracing, struts and trusses.

Fan et al. [9] investigated 36 glued laminated bamboo and laminated veneer lumber composite columns with slenderness ratios ranging from 31.8 to 73.1 and large sectional dimensions. They reported that the ultimate load capacity of composites with thin-strip GLB outer layers increased by 31.6–45.3% compared with those using thick-strip GLB outer layers. Nie et al. [10] examined the influence of slenderness ratio, cross-sectional area, and diameter-to-thickness ratio on the compressive behaviour of natural (non-engineered) bamboo columns. Their results indicated that failure modes were mainly governed by slenderness ratio and diameter-to-thickness ratio. Yu et al. [11] studied the buckling behaviour of structural bamboo with large cross-sections. Verma and Charier [12] analysed the tensile, bending, and compressive properties of laminated bamboo composites, emphasizing the effect of lamination orientation on strength. Yeh and Lin [13] investigated the performance of finger joints in laminated bamboo members under shear, bending, tension, and compression.

Most existing studies on engineered bamboo have focused either on bamboo scrimber [14–16] or bamboo–timber composites such as cross-laminated bamboo-timber [17–19]. Research on the compressive behaviour of GLB is available to some extent, but primarily on large-scale members or small specimens with limited slenderness variations. Systematic studies on GLB covering a broad spectrum of slenderness ratios remain scarce. Moreover, the effects of geometric parameters such as length-to-width ratio, length-to-depth ratio, and slenderness ratio in smaller cross-section GLB members are rarely addressed.

Design codes such as Eurocode 5 [20], the National Design Specification (NDS) [21], and the Chinese code [22] provide analytical methods to predict the strength of timber columns and glued laminated timber. Chen et al. [23] applied these approaches to bamboo scrimber and bamboo scrimber–timber composite columns, while Fan et al. [9] used them to predict the strength of GLB–laminated veneer lumber composite members. Wang et al. [24] examined the mechanical behaviour of cross-laminated timber–bamboo short columns under axial compression and employed these models for prediction. However, the application of these analytical models to pure GLB members across a wide range of slenderness ratios has not been adequately explored, highlighting another significant research gap.

Traditionally, raw bamboo culms have been used as top chords, bottom chords, and web members in roofs. However, due to inherent limitations such as hollow geometry and thin walls, the use of engineered bamboo in truss systems has become increasingly prevalent [25]. Slender glued laminated bamboo (GLB) members, with cross-sectional dimensions up to 50 mm and lengths around 700 mm, are now commonly utilized in trusses. Villegas et al. [26] investigated the design and structural performance of trusses assembled with culms and slats of Guadua angustifolia. Wang et al. [27] introduced a novel joint using nailed Glubam-plate connectors for laminated bamboo lumber (LBL) trusses, experimentally testing their performance under various loading conditions and web configurations. Shi et al. [28] examined bolted connections in GLB roof trusses, focusing on the mechanical behaviour of bamboo-based joints. Ma et al. [29] investigated thin-walled steel–laminated bamboo truss beams and demonstrated, through four-point bending tests, that the use of plain-pressed laminated bamboo lumber as web members significantly enhanced the bending resistance. Beyond truss systems, slender GLB compression elements have potential applications in bracing and struts, small columns and posts, panel stiffeners, furniture components (e.g., chair and table legs, bed frames, sofa supports), shelving uprights, formwork bracing, housing studs, scaffolding, temporary frames, architectural partitions, balustrades, ceiling and wall grids, sports equipment supports, instrument stands,

tripods, and eco-friendly packaging frames [17,30–33]. Despite these widespread applications, comprehensive studies on the compression behaviour of such small-section GLB elements remain limited.

To address these gaps, the present study investigates 84 GLB compression elements with three different cross-sections and varying lengths. The specific objectives are:(a) to examine the stress–strain behaviour and failure modes of GLB specimens under compression across a wide range of slenderness ratios (5–130); (b) to evaluate size effects and the variation of maximum load capacity and compressive strength with respect to different slenderness parameters (length/width, length/depth, and slenderness based on radius of gyration) and stability factors; (c) to perform statistical analysis of variance (ANOVA) to identify parameters significantly affecting GLB compression performance and to develop empirical regression models for accurate load and strength prediction; (d) to conduct theoretical analyses of GLB compression behaviour using GB 50005, Eurocode 5, and the National Design Specification (timber-based standards), and to assess their applicability and deviations when extended to GLB; and (e) to apply the Popovics and Richard–Abbott models for predicting the complete stress–strain behaviour of small-section GLB specimens under compression.

2 Materials and Methods

2.1 Materials

The glued laminated bamboo (GLB) members used in this study were manufactured from mature bamboo culms, which were split into strips and processed to enhance dimensional uniformity and stability.

Fabrication of the GLB members was carried out using hot-pressing under a pressure of 50–90 kgf/cm², depending on the density of the bamboo product. Dynea phenolic resin (DZT-5), a thermosetting adhesive specifically developed for bonding bamboo products, was used. The laminates were pressed at approximately 130 °C for 25 minutes, with minor adjustments to pressing parameters made according to seasonal conditions. All specimens were manufactured in China using Moso bamboo and were supplied by House of Bamboo (Australia). Bamboo fibres were aligned longitudinally and parallel to the loading direction. The bamboo strips used in GLB manufacturing are illustrated in **Fig. 5** (Section 3.1). All specimens were produced with a consistent internal structure to ensure that compressive performance was not influenced by variations in specimen construction.

2.2 Methods

2.2.1 Compression tests on GLB

The experimental program followed ISO 23478 [34]. The bamboo strips in the GLB specimens were oriented longitudinally along the specimen axis. Moisture content was determined immediately after each mechanical test, with the number of readings equal to three times the number of specimens. Measurements were taken from the entire specimen, both before and after loading, using a moisture meter. For each specimen, three readings were taken near the failure zone, and the mean value was reported. Density was calculated by measuring specimen dimensions at three positions along the length (L), width (b), and depth (h); the mean values were used in the calculation. Here, b represents the smaller cross-sectional dimension (**Fig. 1**). All specimens were conditioned prior to testing in a controlled environment of 23 °C and 65% relative humidity. The end-grain surfaces were carefully prepared to ensure that they were plane, parallel, and perpendicular to the specimen axis. For short compression elements (slenderness ratio $\lambda \leqslant 17$), deformation was measured over a central gauge length equal to four times the smaller cross-sectional dimension, in accordance with ISO 23478. For specimens with $\lambda > 17$ (slender compression members), this approach was not adopted. Instead, deformation was measured within a central region located at least one times the larger cross-sectional dimension away from each contact surface, in accordance with ASTM D198 [35], as the ISO 23478 approach does not adequately capture deformation effects in slender elements. Loading was applied at a constant rate to achieve total test durations between 180 and 300 seconds, in accordance with ISO 23478. For this purpose, preliminary tests were conducted to determine an appropriate loading rate. An overall loading

rate of 2.5 mm/min was found to be suitable to ensure that the tests were completed within this duration. The modulus of elasticity, and compressive strength were calculated using Eq. (1) to (2).

$$E_{c,0} = \frac{l_g\left(p_{40} - p_{10}\right)}{bh\left(\delta_{40} - \delta_{10}\right)} \tag{1}$$

$$f_{c,0} = P_{max} / (bh) \tag{2}$$

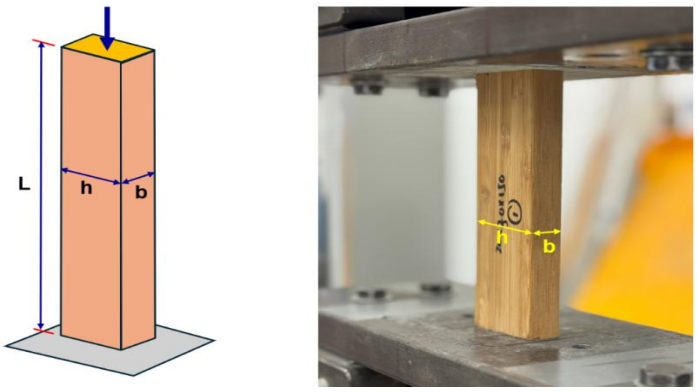

Fig. 1. Test setup for GLB specimen under axial compression.

Table 1. Dimensions of test specimens (coefficient of variation in parentheses).

Specimen	Repetitions	Density (ρ)	MC	*b*	*h*	*L*
-	-	kg/m^3	%	mm	mm	mm
1	3	633.87 (4.58)	9.90 (8.75)	20	20	50
2	3	569.18 (10.29)	10.33 (6.22)	20	20	100
3	3	628.54 (17.01)	9.73 (8.62)	20	20	150
4	3	718.96 (1.00)	8.67 (4.80)	20	20	200
5	3	684.52 (7.88)	9.07 (7.83)	20	20	250
6	3	625.73 (3.95)	8.27 (9.16)	20	20	300
7	3	681.31 (11.18)	8.83 (12.11)	20	20	350
8	3	706.31 (1.38)	9.13 (9.61)	20	50	150
9	3	693.05 (3.62)	9.97 (6.37)	20	50	250
10	3	675.65 (6.65)	8.67 (6.56)	20	50	350
11	3	634.76 (7.99)	8.73 (9.94)	20	50	450
12	3	665.82 (5.33)	8.50 (3.30)	20	50	550
13	3	665.96 (4.24)	8.50 (7.35)	20	50	650
14	3	664.66 (9.18)	8.50 (13.10)	20	50	750
15	3	612.44 (5.09)	8.00 (3.00)	30	38	100
16	3	726.53 (3.40)	7.53 (6.68)	30	38	200
17	3	720.37 (6.78)	10.80 (9.60)	30	38	300
18	3	740.20 (7.27)	7.50 (7.17)	30	38	400
19	3	593.73 (5.46)	9.40 (12.31)	30	38	500
20	3	624.86 (9.84)	8.30 (11.04)	30	38	600
21	3	604.56 (0.56)	9.40 (9.46)	30	38	700
22	3	608.24 (3.31)	6.57 (12.21)	20	50	50
23	3	635.20 (10.81)	8.32 (7.04)	20	20	75
24	3	589.21 (0.42)	9.62 (9.36)	30	38	112.5
25	3	701.09 (2.09)	9.40 (9.31)	20	50	75
26	3	653.61 (4.02)	8.32 (10.04)	20	20	35
27	3	747.86 (0.88)	9.25 (8.46)	30	38	45
28	3	694.14 (0.79)	9.34 (7.36)	20	50	35

Where P_{40} and P_{10} are the applied loads at 40% and 10% of the maximum load (P_{max}), and δ_{40} and δ_{10} are the corresponding displacements. l_g is the gauge length, and *b* and *h* are the cross-sectional dimensions of the specimen. The densities of the GLB specimens ranged from 505.10 to 754.40 kg/m³, with a coefficient of variation (*COV*) of 8.87%. The specimen dimensions and corresponding densities are listed in **Table 1**. These densities were calculated at the moisture contents indicated in the table.

2.2.2 Bending tests on GLB

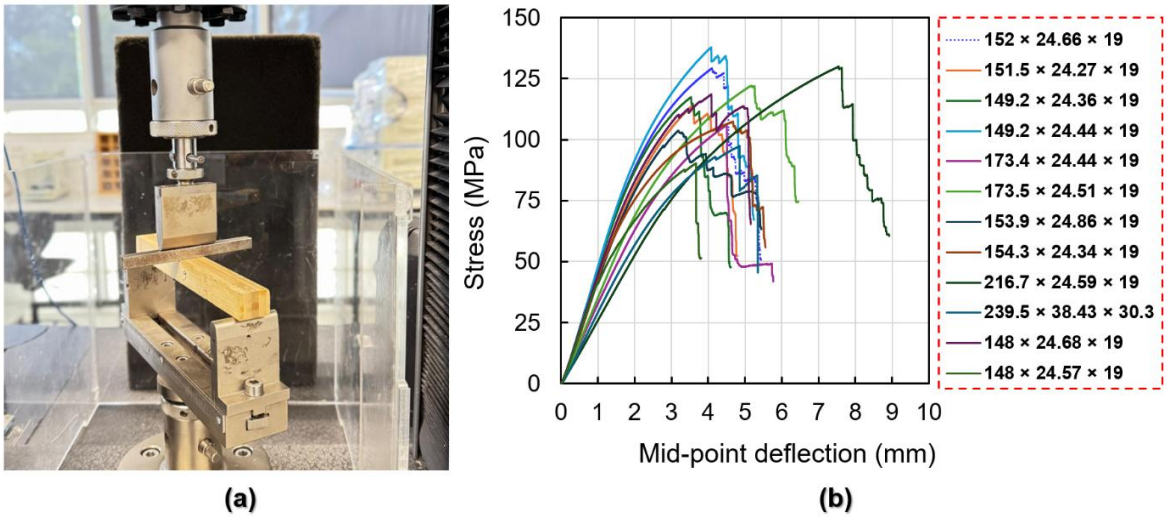

Fig. 2. (a) Test setup for GLB bending, (b) Force–deformation curves from bending tests

Table 2. Key results from bending tests on GLB

ID	L_t	*b*	*h*	*MC*	l_c	ρ	P_{max}	*MOR*	E_b
	mm	mm	mm	%	mm	kg/m^3	kN	MPa	MPa
1	152	24.66	19	9.64	130	703.47	5.90	129.30	9279.6
2	151.5	24.27	19	9.54	130	717.14	5.14	114.30	8368.8
3	149.2	24.36	19	7.32	130	739.69	5.29	117.40	9340.8
4	149.2	24.44	19	8.35	130	726.30	6.23	137.76	9755.9
5	173.4	24.44	19	9.19	160	615.75	3.89	105.76	8708.2
6	173.5	24.51	19	9.03	160	683.07	4.50	122.04	9686.1
7	153.9	24.86	19	8.87	130	656.46	4.77	103.67	8035.8
8	154.3	24.34	19	8.71	130	621.24	4.84	107.35	8314.0
9	216.7	24.59	19	8.55	200	718.26	3.85	129.95	10662.3
10	239.5	38.43	30.3	8.55	200	609.58	11.45	97.33	8512.1
11	148	24.68	19	7.89	130	730.55	5.42	118.53	8550.3
12	148	24.57	19	8.23	130	722.96	4.10	90.24	8225.9
Average				8.65		687.04		114.47	8953.3
COV %				7.69		7.08		12.38	8.84

A total of 12 GLB specimens with varying dimensions and lengths were tested in bending to determine the modulus of rupture (*MOR*) and the modulus of elasticity in bending (E_b), which is typically used in structural design. The test setup and corresponding stress–deformation curves are shown in **Fig. 2**. All tests were conducted in accordance with ISO 23478, with loading durations maintained between 180 and 300 s as recommended. A loading rate of 1.5 mm/min was selected to ensure that the tests were completed within this specified duration. A small steel block (8 × 8 mm) was placed between the circular loading head and the specimen surface to prevent local indentation. The values of E_b and *MOR* were calculated using Eq. (3) and (4), in accordance with ASTM D198. Here, L_t is the total specimen length, l_c is the span length (distance between supports), ρ is the density at the measured moisture content (*MC*), and *h* is the specimen depth. The shear modulus, *G*, was taken as 900 MPa following [36]. E_b represents the shear-free modulus of elasticity. Shear-free means that all deformation is due to bending, with little or no contribution from shear. *P* denotes the applied load, and δ is the displacement within the elastic range. The resulting values are summarized in **Table 2**. With respect to failure modes, all specimens failed in tension. A detailed discussion of the bending results is presented in Section 6.6.

$$MOR = 3P_{max}l_c / (2bh^2) \tag{3}$$

$$E_b = \frac{Pl_c^2}{4bh^3[1-3pl_c/(10bhG\delta)]} \tag{4}$$

3 Results and Discussion

3.1 Failure modes

The slenderness ratio groupings, which distinguish between short and long columns, are discussed in greater detail in the following section and are introduced here to aid interpretation. Based on this classification, specimens with a slenderness ratio of $\lambda \leqslant 17$ are considered short compression elements, those with $\lambda \geqslant 38$ are classified as long compression elements, and specimens with intermediate slenderness ratios fall between these limits [34,35].

The primary failure mode observed in long GLB elements was tensile failure, as shown in **Fig. 3**. In some specimens, buckling occurred in combination with splitting. The slender geometry of these elements made them susceptible to Euler-type buckling. Longitudinal cracks along the laminations indicate that compressive stresses exceeded the shear strength parallel to the grain. Similar to timber, bamboo exhibits low shear strength along the fibre direction, so lateral stresses induced by buckling initiated splitting.

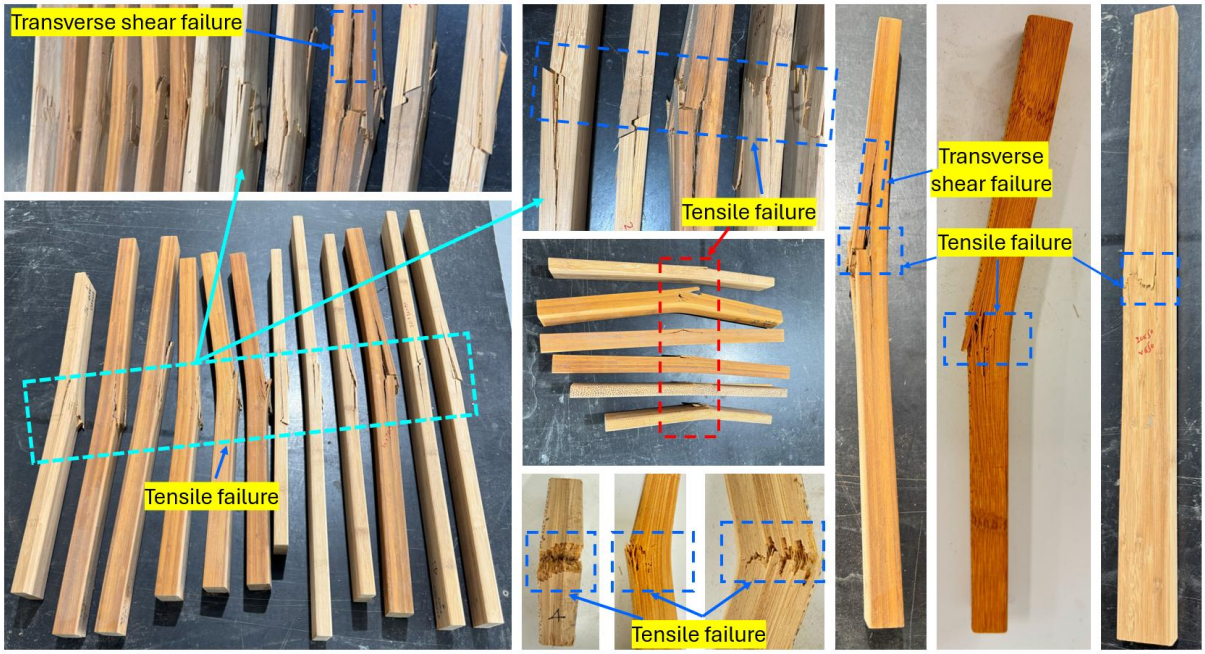

Fig. 3. Failure modes of long GLB compression elements with slenderness ratio ($\lambda \geq 38$)

Long specimens did not fail purely by crushing, which would be characterized by compacted and shortened fibres. Instead, buckling generated tensile stresses on one side and compressive stresses on the opposite side, resulting in cracks along the fibre direction. Overall, the failure mode was mixed: primarily flexural buckling accompanied by shear and tensile splitting along the fibres. In most specimens, failure occurred in the bamboo substrate or fibres rather than in the adhesive, indicating that the bonding was effective. These failure modes can be categorized into three distinct types, as illustrated in **Fig. 4**.

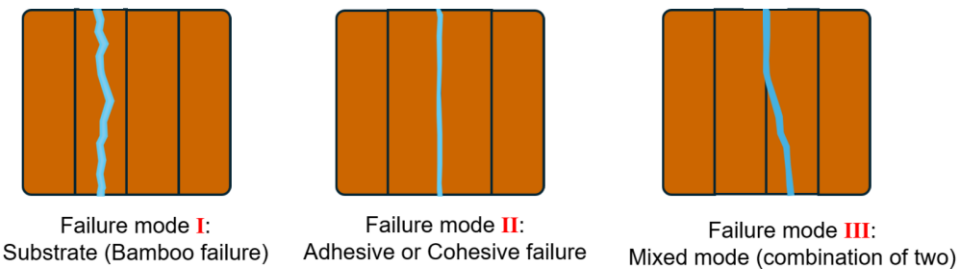

Fig. 4. Types of failure modes in GLB specimens: bamboo failure, adhesive/cohesive failure, and mixed mode.

To determine whether failure occurred within the bamboo or at the adhesive interfaces, the end

sections of all tested specimens were carefully examined. Three possible failure modes were identified, and previously reported by [37]. The marking of these failure modes is shown in **Fig. 5**. Of the 84 specimens, 66 exhibited complete substrate (bamboo) failure. Four specimens failed in Mode II due to adhesive or cohesive failure, representing only 4.80% of the total. Fourteen specimens exhibited Mode III mixed failure, comprising approximately 70% bamboo failure and 30% adhesive failure. These results indicate that most specimens (95.2%) failed within the bamboo substrate Mode I, which is desirable, as the adhesive bonds remained intact.

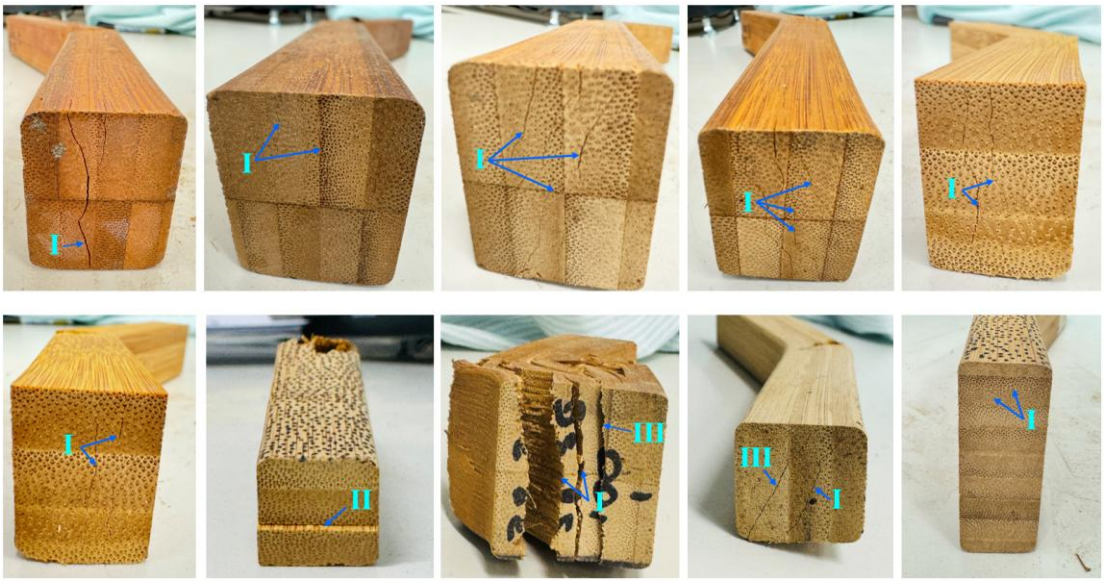

Fig. 5. Failure modes observed at the end sections of GLB compression elements.

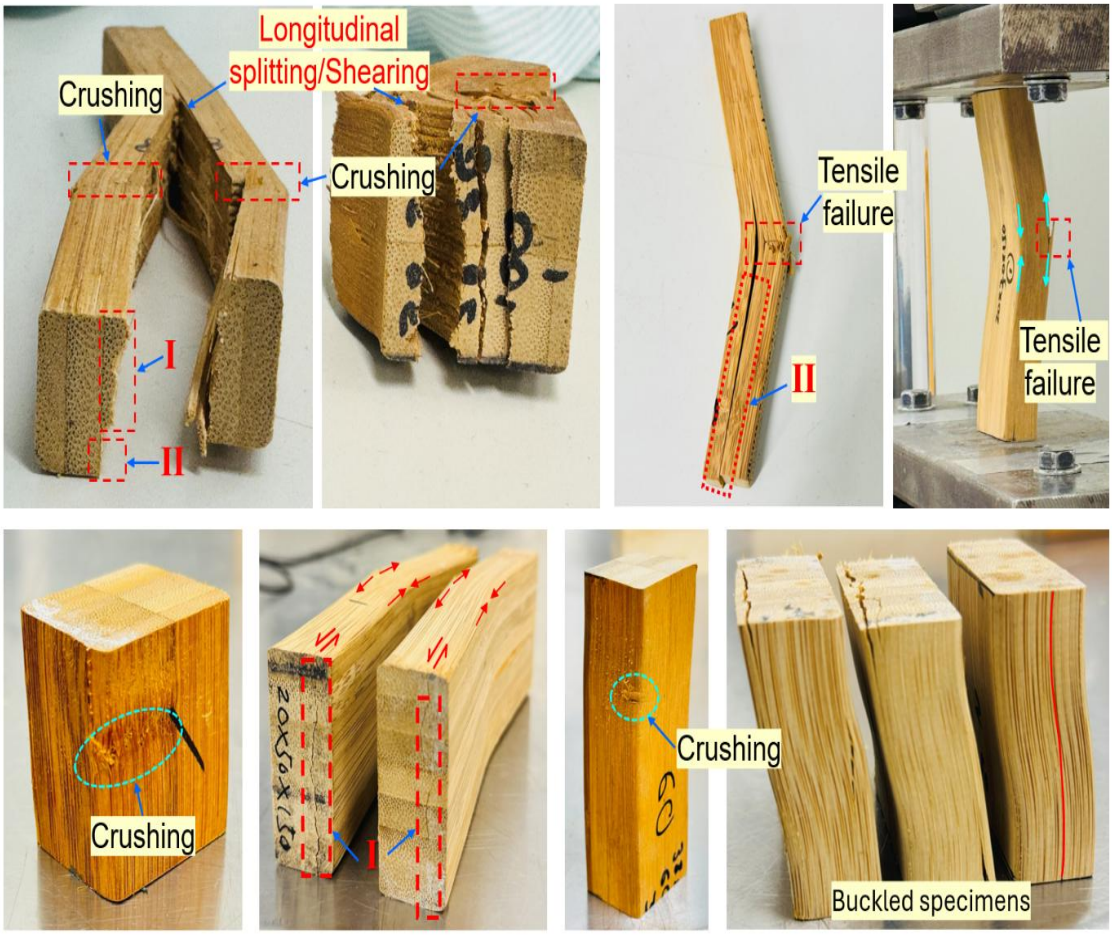

Fig. 6. Failure modes of short GLB compression elements with slenderness ratio ($\lambda \leq 17$)

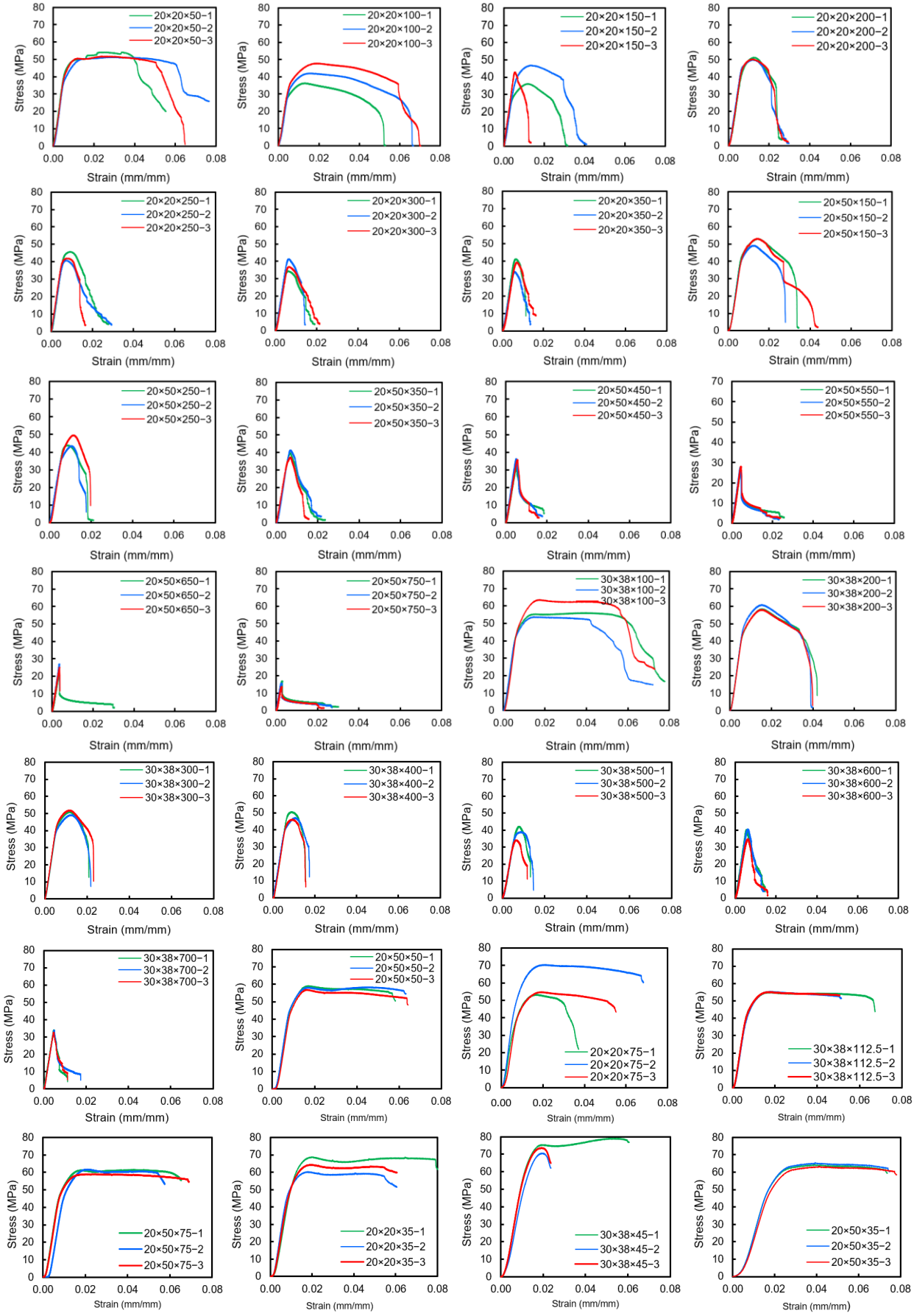

Fig. 7. Stress–strain curves of GLB specimens under axial compression

For short or stocky specimens, the primary failure mode was crushing, often followed by the formation of longitudinal cracks (**Fig. 6**). In some specimens, end splitting was observed at later stages of displacement. Specimens with slenderness ratios (λ) between 8 and 12 experienced some buckling, while those with λ between 12 and 17 exhibited buckling followed by tensile failure. All these failures occurred near the maximum load capacity of the specimens. Later displacement increments also caused end cracking in both short and long columns, which can be attributed to transverse shear deformation. In most cases, cracks propagated through the bamboo substrate rather than the adhesive layer, indicating effective bonding. A few specimens exhibited Mode II failure, as shown in **Fig. 6**.

3.2 Stress-Strain Behaviour

The stress–strain curves for all tests are presented in **Fig. 7**. For members with $\lambda \geqslant 38$, the first region is the elastic region, followed by the peak load and then a softening (descending) region, and failure is dominated by buckling accompanied by tensile cracking. The ductility of the specimens decreases with increasing λ, although the initial slope of the curve remains similar; specimens with higher slenderness ratios exhibit more brittle post-peak behaviour.

Table 3. Key results from compression stress–strain curves (coefficient of variation in parentheses)

Specimens	λ	P_{max}	f_c	E_c	Slenderness ratio grouping
-	-	kN	MPa	MPa	-
30x38x45	5.51 (2.27)	74.82 (6.86)	65.63 (6.86)	6848.57 (6.81)	
20x20x35	5.98 (0.79)	25.74 (6.61)	64.34 (6.61)	7508.91 (6.21)	
20x50x35	6.71 (0.00)	64.25 (1.56)	64.25 (1.56)	7141.76 (0.38)	
20x20x50	8.66 (0.20)	20.98 (2.90)	52.45 (2.90)	8482.18 (2.55)	
20x50x50	9.01 (2.85)	57.98 (1.91)	57.98 (1.91)	7902.43 (2.19)	Short
30x38x100	11.55 (0.52)	65.74 (9.14)	57.67 (9.14)	8639.39 (1.31)	
20x50x75	12.79 (0.85)	60.68 (2.47)	60.68 (2.47)	7626.62 (2.88)	
30x38x112.5	13.51 (1.61)	62.77 (0.34)	55.06 (0.34)	7893.35 (1.83)	
20x20x75	13.56 (0.77)	23.75 (15.98)	59.37 (15.98)	7754.19 (3.50)	
20x20x100	17.32 (0.11)	16.80 (13.71)	42.00 (13.71)	8198.56 (0.37)	
30x38x200	23.09 (0.79)	67.17 (2.53)	58.92 (2.53)	8560.46 (1.28)	
20x20x150	25.98 (0.14)	16.80 (12.97)	42.01 (12.97)	7956.29 (1.26)	
20x50x150	25.98 (0.70)	51.62 (4.43)	51.62 (4.43)	7871.19 (3.48)	Intermediate
20x20x200	34.64 (0.87)	20.17 (1.36)	50.43 (1.36)	7982.10 (0.21)	
30x38x300	34.64 (1.00)	57.60 (2.76)	50.52 (2.76)	8383.14 (0.45)	
20x20x250	43.30 (0.64)	17.09 (6.06)	42.72 (6.06)	8148.43 (2.00)	
20x50x250	43.30 (0.80)	45.56 (7.48)	45.56 (7.48)	7462.60 (3.12)	
30x38x400	46.19 (1.38)	54.40 (4.86)	47.72 (4.86)	7837.40 (1.95)	
20x20x300	51.96 (1.20)	14.96 (9.59)	37.39 (9.59)	7492.41 (4.97)	
30x38x500	57.74 (1.42)	43.67 (10.50)	38.31 (10.50)	7022.66 (0.51)	
20x20x350	60.62 (1.32)	15.21 (10.03)	38.02 (10.03)	7346.24 (7.98)	
20x50x350	60.62 (0.97)	39.33 (5.13)	39.33 (5.13)	7381.67 (3.34)	Long
30x38x600	69.28 (2.13)	43.83 (8.41)	38.45 (8.41)	7696.77 (6.79)	
20x50x450	77.94 (1.23)	34.38 (7.47)	34.38 (7.47)	7237.19 (5.00)	
30x38x700	80.83 (0.76)	38.00 (2.32)	33.33 (2.32)	7504.14 (2.33)	
20x50x550	95.26 (1.63)	27.16 (3.73)	27.16 (3.73)	6950.92 (3.25)	
20x50x650	112.58 (1.43)	24.28 (12.81)	24.28 (12.81)	7251.71 (4.81)	
20x50x750	129.90 (2.27)	15.32 (10.81)	15.32 (10.81)	7111.84 (3.06)	

However, for specimens with slenderness ratios of $\lambda \leqslant 17$, which primarily failed by crushing accompanied by moderate splitting and shear, the stress–strain behaviour can be divided into four distinct regions. The first region is the elastic region, where the modulus of elasticity (*MOE*) is calculated and no visible damage is observed. The second region is the non-linear hardening stage, also referred to as the post-elastic region, in which the curve deviates from linearity. During this stage, micro-cracks and local crushing of bamboo fibres begin. Stress continues to increase, but with reduced stiffness, reflecting the ability of bamboo fibres and the matrix to redistribute stresses. The third region

corresponds to plasticity, where stress remains nearly constant while bamboo fibres and parenchyma cells undergo micro-crushing and densification. The material does not fail immediately; it sustains additional strain while maintaining high stress. Visually, specimens exhibit end crushing and gradual splitting. The peak stress typically occurs within this plastic region. The final region is softening or descending, where crushing spreads and longitudinal cracks propagate. Unlike slender columns, the stress drop is gradual, indicating post-peak ductility. Residual strength is maintained due to friction and compaction of crushed fibres.

Key results obtained from the stress–strain curves are summarized in **Table 3**. It is observed that the modulus of elasticity in compression (E_c) decreases with increasing slenderness ratio, likely due to buckling and instability effects that reduce the apparent stiffness. Specimens that reached their full load capacity exhibited a compressive strength (f_c) of approximately 65.63 MPa and E_c of around 8400 MPa. The slenderness ratio (λ) of the tested specimens ranged from 5.51 to 129.90, with corresponding maximum loads (P_{max}) and compressive strengths varying from 15.32 kN (15.32 MPa) to 74.82 kN (65.63 MPa), respectively.

4 Statistical study

4.1 Best Subsets Regression and Analysis of Variance (ANOVA)

Table 4. Best Subsets Regression for Identifying the Most Predictive Regression Models

Response is f_c											
Vars	R-Sq	R-Sq (adj)	R-Sq (pred)	Mallows *Cp*	*S*	*b*	*h*	*L*	*ρ*	*λ*	*V*
1	84	83.8	83.3	86.1	5.20					X	
1	74	73.7	72.6	191.3	6.62			X			
2	89.8	89.6	89	26.5	4.17				X	X	
2	86.5	86.2	85.5	61.5	4.80		X			X	
3	91.7	91.4	90.9	8.7	3.79				X	X	X
3	**91.4**	**91.1**	**90.5**	**11.8**	**3.86**		**X**		**X**	**X**	
4	92.3	92	91.4	3.9	3.66		X		X	X	X
4	92.3	91.9	91.4	4.6	3.68			X	X	X	X
5	92.4	91.9	91.1	5.4	3.67		X	X	X	X	X
5	92.3	91.9	91.1	5.7	3.68	X	X		X	X	X
6	92.4	91.8	91	7	3.69	X	X	X	X	X	X
Response is P_{max}											
Vars	R-Sq	R-Sq (adj)	R-Sq (pred)	Mallows Cp	*S*	*b*	*h*	*L*	*ρ*	*λ*	*V*
1	34.2	33.4	31.4	3227.2	15.7	X					
1	30.4	29.5	27.7	3418.1	16.2		X				
2	70.9	70.2	69.3	1384.1	10.5		X			X	
2	61.1	60.2	58.4	1872.5	12.1			X			X
3	96.3	96.1	95.8	108.5	3.8	X	X				X
3	96	95.8	95.6	123.8	3.9	X	X	X			
4	**97.4**	**97.3**	**97.1**	**52.8**	**3.2**	**X**	**X**		**X**	**X**	
4	97.3	97.1	96.9	60.6	3.3	X	X	X	X		
5	98.1	98	97.8	19.9	2.7	X	X		X	X	X
5	97.6	97.5	97.3	45	3.1	X	X	X	X	X	
6	98.4	98.3	98.1	7	2.5	X	X	X	X	X	X

Best Subsets Regression (BSR) is a statistical method used to identify the most predictive regression models by evaluating all possible combinations of specified predictors. In this study, models including multiple predictors (b, h, L, ρ, λ, V) were assessed, and those with the highest R^2 were considered the best fitting. By selecting only the most relevant subset of predictors, BSR can produce models with lower variance in coefficient estimates and improved predictive accuracy compared to models that include all predictors. This method efficiently identifies the key variables that most strongly influence the response, enhancing both interpretability and model reliability. The results of the BSR are

presented in **Table 4**. Here, Mallows' Cp is a statistic used to assess model fit; models with Cp close to the number of predictors plus one are considered optimal, with lower values indicating a better balance between bias and variance. *S* represents the standard deviation of the residuals (standard error of the regression), where smaller values indicate a better fit. *Vars* denotes the number of predictors included in the model, and *V* is the volume of GLB specimen. Based on this analysis, the parameter models highlighted in bold were selected for subsequent ANOVA analysis. These selected models use fewer parameters while achieving relatively lower *S* and *Cp* values and high R^2, indicating a favourable balance between accuracy and simplicity.

ANOVA was conducted using Minitab statistical software to identify trends, predict patterns, and uncover relationships between variables. The ANOVA results for maximum load (P_{max}) and compressive strength (f_c) are presented in **Table 5**. The table includes degrees of freedom (*DF*), adjusted sum of squares (*Adj SS*), and adjusted mean squares (*Adj MS*). Of particular importance are the F-values and P-values: a higher F-value indicates a stronger effect of the factor on the response variable, while a small P-value (typically < 0.05) indicates statistical significance. Less significant parameters were excluded from the analysis.

Table 5. ANOVA for the response variables: P_{max} and f_c.

P_{max}					
Source	DF	Adj SS	Adj MS	F-Value	P-Value
Regression	4	31017.1	7754.3	773.8	0.000
b	1	7985.2	7985.2	796.8	0.000
h	1	13574.1	13574.1	1354.5	0.000
ρ	1	585.6	585.6	58.4	0.000
λ	1	10598.0	10598.0	1057.6	0.000
Error	82	821.7	10		
Total	86	31838.9			
f_c					
Source	DF	Adj SS	Adj MS	F-Value	P-Value
Regression	3	13090.6	4363.5	293.5	0.000
h	1	226.6	226.6	15.2	0.000
ρ	1	702.0	702.0	47.2	0.000
λ	1	11706.9	11706.9	787.3	0.000
Error	83	1234.2	14.9		
Total	86	14324.8			

For the P_{max} response variable, the overall model was highly significant, with F = 773.8 and P = 0.000, indicating that the predictors (b, h, λ, ρ) collectively explain a substantial portion of the variation in maximum load. The model accounts for 97.42% of the variability, demonstrating an excellent fit. Among the predictors: Cross-sectional width (b) has F = 796.8 and P = 0.000, showing strong significance. Bamboo member depth (h) is the most influential factor, with F = 1354.5 and P = 0.000. Changes in depth significantly affect P_{max}, as low depth increases susceptibility to buckling. Depth can thus be considered a key design parameter. Slenderness ratio (λ) is also highly significant, with F = 1057.6 and P = 0.000. Density (ρ) shows a statistically significant influence on P_{max}; higher density correlates with greater strength, consistent with typical behaviour of biomaterials. For compressive strength (f_c), the regression model using depth (h), density (ρ), and slenderness ratio (λ) as predictors is highly significant, with an overall F = 293.5 (P < 0.001). The model explains 91.39% of the total variation in f_c, indicating strong predictive capability. Among the variables, slenderness ratio dominates the regression variability (F = 787.3, P < 0.001), confirming that geometric instability and buckling primarily govern compressive strength. Density is also significant (F = 47.2, P < 0.001), but its contribution is smaller, indicating that higher material density improves strength to a lesser extent than geometry. Depth (h) contributes moderately to f_c. The term "Error" denotes the unexplained variation not accounted for by the regression model. Its relatively small magnitude compared to the explained variation indicates good agreement between the model predictions and the experimental data. The empirical regression equations derived for P_{max} and f_c (Eq. (5) and (6)) yield R^2>0.90 (**Fig. 8**), demonstrating excellent predictive accuracy. Unlike previous empirical models in the literature for bamboo products, which consider only geometric parameters, these equations also account for material

density, enhancing prediction reliability.

$$P_{max,emp} = -63.10 + 2.0840b + 1.0749\rho - 0.3553\lambda \quad (5)$$

$$f_{c,emp} = 24.26 + 0.1384h + 0.04953\rho - 0.3717\lambda \quad (6)$$

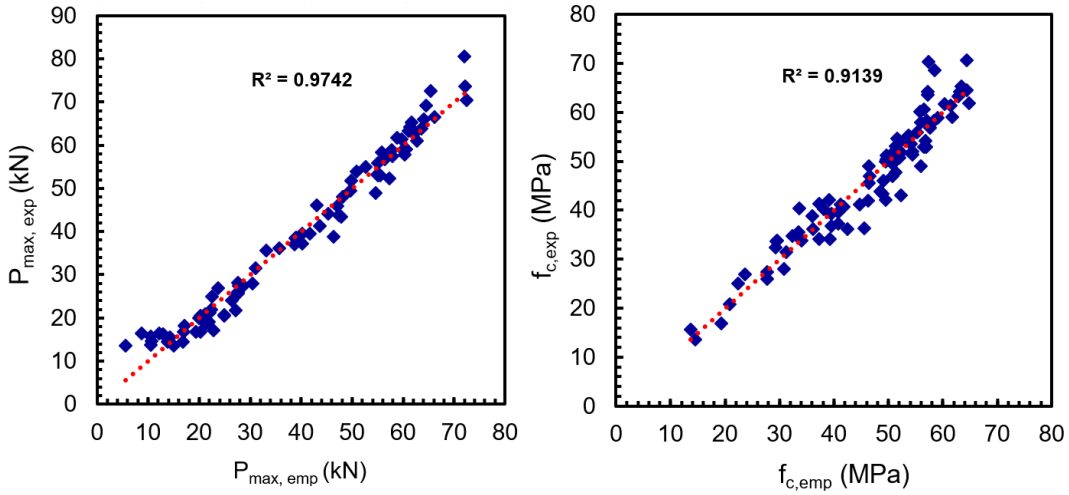

Fig. 8. Comparison of experimental and empirically predicted values of P_{max} and f_c.

5 Effect of Size and Slenderness Ratio

5.1 Effect of slenderness: Column types

Short compression elements are characterized by a fully non-linear material stress–strain response in compression. As the slenderness ratio (λ) increases, the failure mode gradually becomes less dependent on material properties and more influenced by geometric effects and instabilities. According to ASTM D198 [35], columns with λ<17 are classified as short columns and are expected to reach their axial capacity. The same definitions are adopted in this study in line with ISO standards. A common formulation defines a long column as one whose λ exceeds the elastic threshold λ_y, given by:

$$\lambda_y = \pi\sqrt{E / f_y} \quad (7)$$

According to this classification, compression specimens with λ<17 are considered short, those with λ>38 are long, and specimens with intermediate values fall in between. However, experimental observations indicate that these limits may vary slightly depending on failure modes. For example, specimens with λ up to approximately 25 primarily exhibited crushing accompanied by shear and splitting, which aligns with the behaviour of short members. Specimens with λ>55 failed by Euler buckling about the weak axis, followed by tensile failure on the convex side at mid-height, with minimal or no material crushing; failure was sudden in these cases.

In this study, the limits of λ=17 and λ=38 are used. Although distinguishing intermediate compression members is challenging, specimens with 17≤λ≤38 can be classified as intermediate columns, typically failing through a combination of material non-linearity and geometric instability. It was also observed that specimens 20×20×150 and 20×50×150, despite having the same λ, exhibited different strengths. This discrepancy can be attributed to the size effect, which is rarely discussed in literature.

5.2 Size effect

The Best Subsets Regression (BSR) results listed in **Table 4** indicate that the volume (V) of bamboo is statistically significant. There are very few studies addressing the size effect in engineered bamboo products. One notable study by Zhao and Zhang (2019) [14] investigated the size effect in bamboo scrimber, while other studies have also reviewed this phenomenon [15]. In the current study, the slenderness ratio (λ) is plotted against the ultimate compressive strength (f_c) in **Fig. 9a**. An increase in λ leads to a reduction in f_c in a linear manner. Additionally, the variability in strength data decreases

with increasing λ; data are more scattered at low λ and more clustered at high λ. Alternatively, in the short compression member range, different strength values were observed at the same or similar λ.

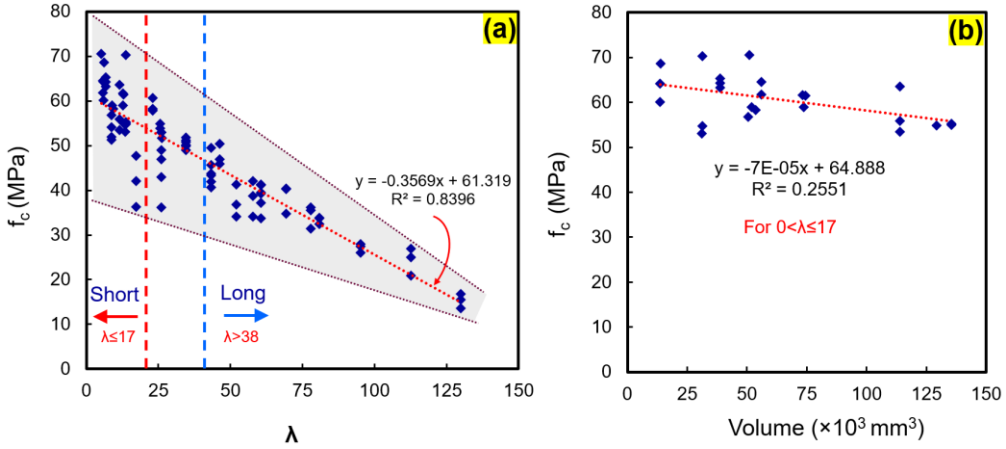

Fig. 9. (a) Slenderness ratio versus ultimate strength; (b) Volume versus ultimate strength.

ISO 23478 recommends a specimen length six times the smaller cross-sectional dimension, corresponding to a column slenderness ratio of 17. This standard effectively categorizes compression specimens with $\lambda \leq 17$ as short columns, expected to reach their full capacity. In this study, 24 specimens with $\lambda < 17$ were tested. The corresponding data are separated and plotted in **Fig. 9b**. For identical λ, similar strength values would be expected; however, variations in f_c were observed. This difference is attributed to the size effect rather than inherent uncertainties in the biomaterial, consistent with findings reported in [15]. For similar λ, the f_c decreases with increasing specimen size. This indicates that, similar to bamboo scrimber, size effects are present in GLB, with strength inversely related to specimen volume. Further studies with larger sectional sizes are recommended to fully substantiate this effect.

5.3 Correlations

The compressive strength (f_c) decreases linearly with increasing L/b ratio, as longer and more slender members are more prone to buckling, thereby reducing their effective load-carrying capacity. A high coefficient of determination (R^2=0.8396) indicates a strong correlation. A significant correlation is also observed between f_c and L/h, though the R^2 value is lower than that for L/b. Since b is the smaller cross-sectional dimension, it governs the buckling behaviour, resulting in the stronger correlation. Experimentally, the stability factor (ϕ) was determined as the ratio of the actual compressive strength to the maximum strength. ϕ decreases almost linearly with increasing slenderness ratio. These results are presented in **Fig. 10**.

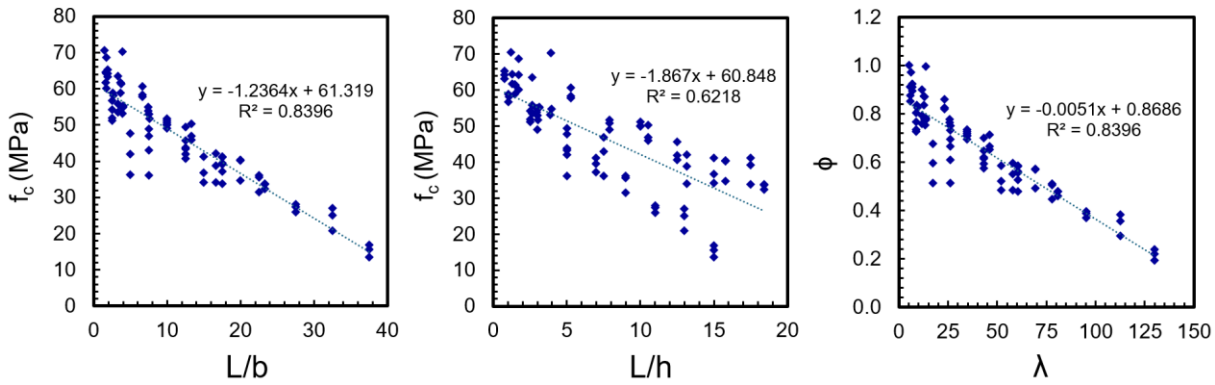

Fig. 10. Relationship of compressive strength (f_c) with L/b and L/h, and stability factor (ϕ) with λ.

The overall trend of compressive strength with respect to the depth-to-width ratio (h/b) shows a decreasing slope, with a slope value of −3.7405, as presented in **Fig. 11**. Specimens with h/b=2.5 exhibited the largest variation in strength. This can be attributed to the wider range of slenderness ratios

in these specimens compared to others. In contrast, square or nearly square specimens tend to show less variation in results, as their symmetry reduces directional effects, leading to more consistent performance. The maximum compressive strengths recorded were 70.29 MPa for specimens with *h/b*=1.0, 70.6 MPa for *h/b*=1.27, and 65.26 MPa for *h/b*=2.5. These results confirm that maximum strength decreases as the h/b ratio increases. However, further studies with a broader range of *h/b* values are recommended to validate this trend. Moreover, in the present study, both cross-sectional dimensions and slenderness ratio vary among specimens, which introduces coupled effects. As a result, it is not always possible to attribute the observed performance differences to a single independent factor. Although the influences of geometric ratios such as *L/b*, *L/h*, and specimen volume on compressive strength were investigated, these parameters inherently incorporate both length and cross-sectional effects, and a complete separation of these influences is limited. Further studies are therefore recommended to more systematically investigate the coupled effects of geometry and slenderness under controlled conditions.

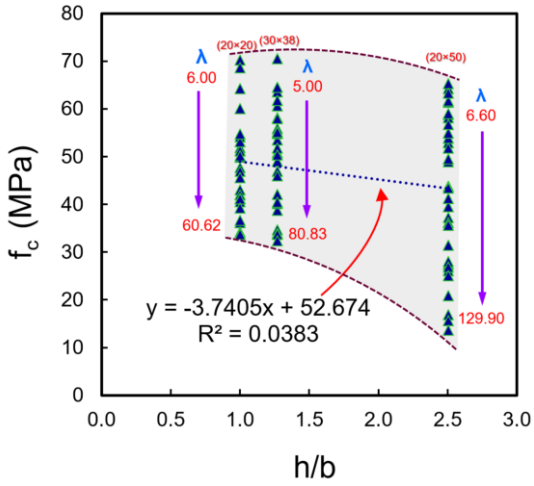

Fig. 11. Effect of depth-to-width ratio on compressive strength for members of various slenderness ratios

6 Theoretical Models and Calculations

In this study, the mean value for each group was obtained from the average of three tests. The experimental results were compared with the design standards GB 50005-2017, Eurocode 5, and NDS. For these model applications, the compressive strength (f_c=65.63MPa) and modulus of elasticity (E_c=8400) were used. These models were originally developed for glued laminated timber but are explored here for GLB.

6.1 Chinese GB code

According to the Chinese GB code [22], the compressive capacity of a glued laminated compression element can be calculated using the following expression:

$$f_{GB,cal} = \varphi f_c \tag{8}$$

where f_c is the design compressive strength of the column parallel to the fibre, and ϕ is the column stability factor, defined as follows:

$$\phi = \frac{a_c \pi^2 \beta E_k}{\lambda^2 f_{ck}} \quad (\lambda > \lambda_c)$$

$$\phi = \frac{1}{1 + \dfrac{\lambda^2 f_{ck}}{b_c \pi^2 \beta E_k}} \quad (\lambda \le \lambda_c) \tag{9}$$

$$where\ \lambda_c = c_c \sqrt{\beta E_k / f_{ck}}$$

where λ is the slenderness ratio, f_{ck} and E_k are the standard values of compressive strength and elastic modulus of the compression element, respectively. β is the correlation coefficient for material shear deformation, while a_c, b_c, and c_c are material correlation coefficients. For glued laminated timber, the values adopted from the GB code are: β=1.05, a_c=0.91, b_c=3.69 and c_c=3.

6.2 Eurocode

According to EC5 [20], the compression capacity of a column is given by:

$$f_{EC5,cal} = \varphi f_{cd} \tag{10}$$

where ϕ is the reduction factor for column stability, defined as:

$$\phi = \frac{1}{k + \sqrt{k^2 - \lambda_{rel}^2}}$$

$$k = 0.5\left[1 + \beta_c \left(\lambda_{rel} - 0.3\right) + \lambda_{rel}^2\right] \tag{11}$$

$$where\ \lambda_{rel} = \frac{\lambda}{\pi}\sqrt{\frac{f_{ck}}{E_k}}$$

Here, f_{cd} is the design compressive strength, λ_{rel} is the relative slenderness ratio, and β_c is a factor accounting for member straightness, taken as 0.1 for glued laminated timber.

6.3 NDS-2018

According to the NDS [21], the axial compression stability coefficient (C_p) is calculated as:

$$c_p = \frac{1 + \frac{F_{cE}}{F_c}}{2c} - \sqrt{\left(\frac{1 + \frac{F_{cE}}{F_c}}{2c}\right) - \frac{\frac{F_{cE}}{F_c}}{c}} \tag{12}$$

$$F_{cE} = \frac{0.822 E_{min}}{\left(l_e / d\right)^2} \tag{13}$$

$$E_{min} = \frac{1.05E\left[1 - 0.645\left(cov_E\right)\right]}{1.66}$$

$$E_{NDS,cal} = f_c C_D C_M C_t C_p \tag{14}$$

Here, c=0.9 for structural glued laminated timber (a non-linear constant), d is the least cross-sectional dimension of a rectangular column, and l_e is the effective column length. C_D, C_M, and C_t are the load duration, wet service, and temperature factors, respectively (taken as 1 here, since these effects are considered normal). C_p is the stability coefficient. For columns with non-rectangular cross-sections, d is replaced by r$\sqrt{12}$, where r is the radius of gyration.

6.4 Calculations

Using the above three models, the peak compressive strength (f_c) of all specimens was predicted, and the results are compared in **Fig. 12**. All three models provide close predictions for members with slenderness ratios up to approximately λ=50. However, at higher slenderness ratios (Region 2 in **Fig. 12**), all models underestimate the strength values. This behaviour may be attributed to the effect of reduced cross-sectional dimensions, where additional safety factors or penalties are inherently applied to slender members. Among the codes, the Chinese code and Eurocode 5 yield nearly identical predictions across the full range of λ, while the NDS provisions are more conservative. On average, the Chinese code underestimates the strength by about 13%, Eurocode 5 by 13%, and the NDS by 27%.

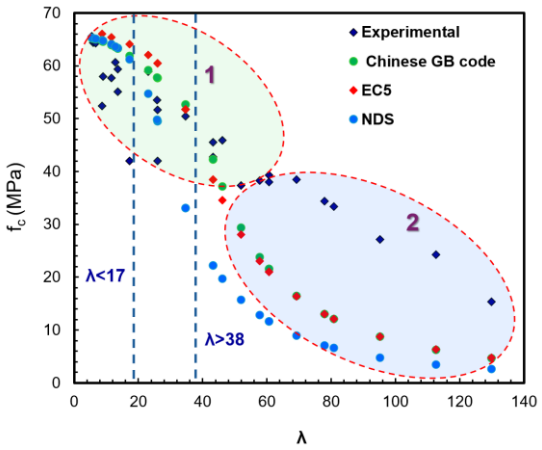

Fig. 12. Comparison of experimental compressive strength values with theoretical model predictions

6.5 Proposed Mathematical Model for Predicting Stress–Strain Curves

Literature studies [38] indicate that when GLB is subjected to tensile loading, the stress–strain relationship is essentially linear and can be expressed by a simple linear equation (the product of elastic modulus and tensile strain), as shown in Eq. (15). In contrast, under compression loading, the stress–strain behaviour of GLB can be divided into four regions, as discussed in the previous sections. These regions include the elastic stage, the elasto-plastic transition stage, and the approximately linear stage after yielding, followed by a softening stage.

The first and third stages of the stress–strain curve can be represented by linear relationships with different slopes. The second stage, or elasto-plastic transition, serves as a link between the first and third stages, ensuring a smooth curve. In this region, once the elastic limit is exceeded, the rate of axial strain growth increases, resulting in a non-linear stress–strain response. In the third stage, axial strain increases rapidly and continuously, while stress either remains nearly constant or increases at a much slower rate. The fourth stage, corresponding to softening, is not considered in this study.

In the literature, several models have been developed to predict the stress–strain behaviour of materials, including the Popovics model [39], the Sargin model [40], and the Richard–Abbott model [41]. Among these, the Richard–Abbott model incorporates the three key stages of the stress–strain curve, as illustrated in **Fig. 13a**. Therefore, this model was adopted in the present study to represent the compressive behaviour of GLB, expressed in the form of Eq. (15).

$$\sigma = \frac{\left(E_c - E_p\right).\varepsilon}{\left[1+\left(\frac{\left(E_c - E_p\right).\varepsilon}{f_o}\right)^n\right]^{\frac{1}{n}}} + E_p.\varepsilon \geq 0 \qquad (15)$$

$$E_p.\varepsilon < 0$$

In this model, the stress σ corresponds to the strain ε, within the range $f_{tu} \leq \sigma \leq f_{cu}$. Here, E_c is the initial elastic modulus obtained from compression testing, and E_p is the post-yield modulus in compression. The parameter n, referred to as the shape factor, characterizes the hardening region. E_t denotes the tensile modulus of elasticity, f_0 is the reference plastic stress, f_{cu} is the ultimate compressive strength, and ε_{cu} is the ultimate compressive strain.

Unlike piecewise formulations, this model provides a continuous representation of the stress–strain curve with a single expression, which is one of its key advantages. The parameter n, which defines the curvature of the curve at the onset of nonlinearity and depends on the experimental behaviour, was set to 3 in the present study for GLB.

For comparison, the Popovics model was also evaluated for GLB. This model requires the strain at maximum strength, ε_0, and is expressed here as Eq. (16).

$$\sigma = \frac{n-1}{n-1+\left(\frac{\varepsilon}{\varepsilon_0}\right)^n} + E_p.\varepsilon \qquad (16)$$

6.5.1 Model predictions

To apply these models, the values of f_c, E_c, and E_p were obtained from the experimental stress–strain curves. For the 20×20×50 mm and 30×38×100 mm specimens, the parameters were determined as: E_c =8000MPa, E_p=2MPa, f_{cu} =56MPa, f_0=55MPa, and n=3. These values were found to be equally applicable to other short specimens. Wei et al. [38] also proposed correlations for GLB, such as E_p=0.04E_c , f_0=0.82f_{cu} , and ε_{cu}=0.050. Using these parameters, the complete stress–strain curve for GLB can be predicted. A comparison between experimental and analytically predicted stress–strain curves is shown in **Fig. 13b**. Both curves are in close agreement in the elastic, hardening, and post-elastic regions, confirming that the proposed model has good applicability for GLB. It should be noted that the mechanical properties of GLB are influenced by the bio composition of the raw bamboo, which in turn depends on factors such as climate, geographical origin, and moisture content. Therefore, regional applicability requires experimental determination of these parameters. While the Popovics model provides good agreement in the elastic and hardening regions, it shows noticeable deviations in the post-hardening stage.

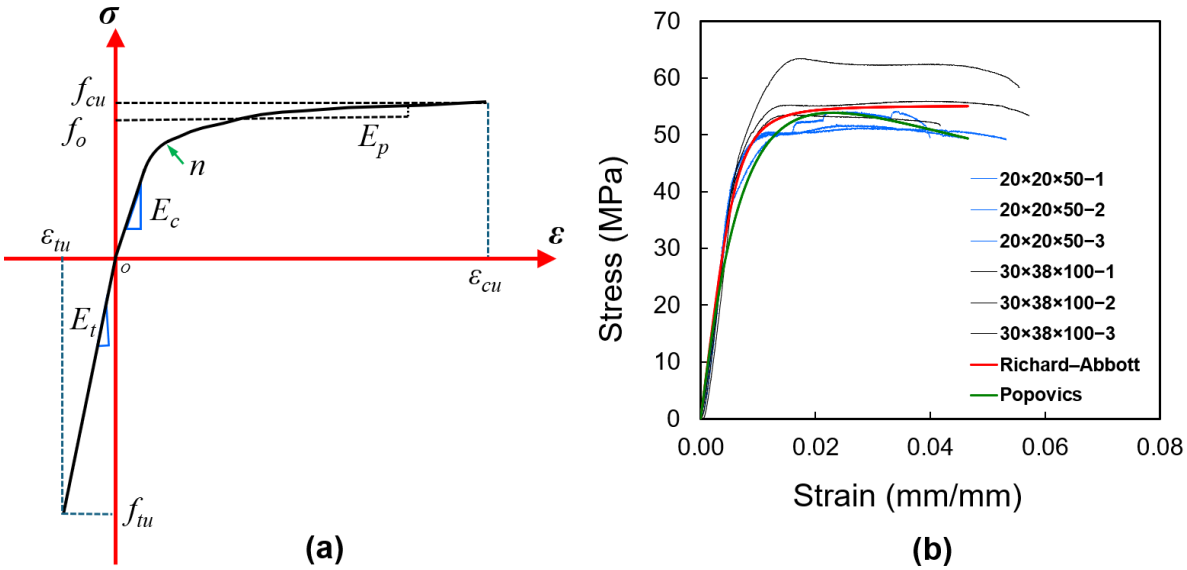

Fig. 13. Proposed model for predicting stress-strain curves of GLB (b) Comparison of experimental and analytical predicted curves.

6.6 Discussion in Australian Context

This study was conducted on GLB specimens sourced from the prominent Australian company House of Bamboo, which specializes in engineered bamboo products for sustainable building applications in Australia.

Australia has a total commercial plantation area of 1.942 million hectares, of which 1.037 million hectares are softwood plantations. More than 80% of Australia's sawlog supply is derived from softwood plantations, with radiata pine accounting for approximately 74% of this volume [42]. The Housing Industry Association (HIA) projects that between 95,000 and 115,000 detached dwellings will be built annually in Australia, with about 75% expected to use timber framing. Demand for sawn softwood is forecast to increase by around 30% by 2050. With the national population expected to reach 35–40 million, overall demand is projected to rise by 40–50%, surpassing current domestic production capacity. According to projections by the Australian Bureau of Agricultural and Resource Economics and Sciences (ABARES), the supply of softwood sawlogs will fall short of demand by approximately 3.4 million m³ by 2050. Machine-graded pine (MGP), particularly MGP10, is the most commonly

available structural softwood in the Australian market and is widely used in load-bearing applications. MGP10 has a modulus of elasticity (E_b) of 10,000 MPa, as specified in AS 1720.1 [43]. This value is comparable to the shear-free modulus of elasticity obtained for GLB in this study (8953.3 MPa), as listed in **Table 2**, showing a difference of approximately 10%. Furthermore, the *MOR* of radiata pine is 80.70 MPa and its compressive strength is 41.9 MPa [44], both of which are lower than the corresponding values measured for GLB, as reported in **Table 2** and **3**, respectively. The other significant favourable characteristic of GLB is negligible distortion and dimensional stability, both of which are critical for future automation in the construction sector. GLB studs can be considered as viable alternative for other imported timber and engineered timber products in light frame construction without affecting the domestic timber market.

7 Conclusions

In this study, 84 GLB elements were tested under axial compression and 12 under bending. The compression data were used to analyse stress–strain behaviour, identify failure modes, develop empirical equations, and predict the maximum strength and stress–strain response of GLB using theoretical approaches. The following key conclusions are drawn:

- The dominant failure mode in GLB elements was buckling, followed by tensile rupture in slender columns. For short or stocky specimens, failure was primarily governed by crushing, often accompanied by longitudinal splitting. The stress–strain response of short specimens exhibited distinct stages: an initial elastic region, a non-linear hardening phase, a plastic plateau where stress remained nearly constant, and a softening or descending branch. In contrast, long columns lacked a distinct plastic region.
- For specimens with similar slenderness ratios (λ), compressive strength (f_c) decreased with increasing specimen size, indicating a pronounced size effect in GLB similar to that reported for bamboo scrimber. Strength was inversely correlated with specimen volume. The compressive strength (f_c) also decreased linearly with increasing L/b and L/h ratios, as slender members were more prone to buckling, reducing their effective load-bearing capacity. Since b is the smaller cross-sectional dimension, the L/b ratio governed buckling behaviour more strongly than L/h. The stability factor (ϕ), defined as the ratio of actual compressive strength to maximum compressive strength, decreased almost linearly with increasing λ.
- Best Subsets Regression and ANOVA revealed that maximum load (P_{max}) was significantly influenced by b, h, ρ, and λ, while compressive strength (f_c) was affected by h, ρ, and λ. The proposed empirical equations for predicting P_{max} and f_c demonstrated high accuracy and reliability.
- Code-based models (GB 50005-2017, Eurocode 5, and NDS) provided reasonable predictions for members with $\lambda \leq 50$. However, at higher slenderness ratios, all models underestimated compressive strength. This underestimation may be attributed to the additional safety factors and penalties embedded in the design provisions for slender members. Among the three codes, the Chinese code and Eurocode 5 produced nearly identical predictions across the full range of λ, whereas NDS predictions were more conservative.
- The Richard–Abbott model was shown to be well-suited for representing the complete stress–strain response of GLB across all stages. The Popovics model provided good agreement in the elastic and hardening regions but deviated considerably in the post-hardening region.
- The bending and compression test results collectively indicate that GLB possesses mechanical properties comparable to, and in some cases superior to, those of commonly used softwood species in Australia (e.g., radiata pine). Therefore, GLB has strong potential to be adopted as a sustainable alternative construction material in the Australian building industry.

Acknowledgement

The authors would like to acknowledge the support of architect Jennifer Snyders, CEO of House of Bamboo, for providing materials and valuable assistance throughout this project. Special acknowledgement to William Hanning, who conducted compression tests on GLB specimens as part of his undergraduate project.

Funding Statement

The author(s) received no specific funding for this study.

CRediT authorship contribution statement

Inayat Ullah Khan: Investigation, Formal analysis, Writing – original draft. **Haitao Li**: Supervision, Investigation, Writing – review & editing. **Mahmud Ashraf**: Supervision, Writing – review & editing.

Conflicts of Interest

The authors declare that they have no conflicts of interest to report regarding the present study.

Data Availability Statement

The data supporting the findings of this study are available from the corresponding author upon reasonable request.

References

[1] Kenney A, Zhang C, Bhandari L, Liang R, GangaRao H. Mechanical response of glass/kevlar hybrid composite jackets for steel containers carrying hazardous materials to enhance safety. Sustain Struct 2024; 4. https://doi.org/10.54113/j.sust.2024.000055.

[2] Mallampati SC, Komal UK, Rakesh P, Barman P. Investigation of the mechanical response of MWCNTs infused carbon/glass fiber-based hybrid composites using digital image correlation. Construction and Building Materials 2025; 492: 143068. https://doi.org/10.1016/j.conbuildmat.2025.143068.

[3] Rubio I, Valverde-Marcos B, Loya JA, Miguélez MH. From low velocity to real ammo impact behaviour of advanced aramid and UHMWPE composites. Thin-Walled Structures 2025; 216: 113715. https://doi.org/10.1016/j.tws.2025.113715.

[4] Khan IU, Subhani M, Ghabraie K, Ashraf M. Exploring and refining testing approaches for hardwood dowels under axial and flexural loading: an experimental and numerical study. Wood Material Science & Engineering 2025; 0: 1–23. https://doi.org/10.1080/17480272.2025.2505135.

[5] Dwivedi AK, Kumar A, Baredar P, Prakash O. Bamboo as a complementary crop to address climate change and livelihoods – Insights from India. Forest Policy and Economics 2019; 102: 66–74. https://doi.org/10.1016/j.forpol.2019.02.007.

[6] Khan IU, Subhani M, Ghabraie K, Ashraf M. Mechanical performance and design challenges of wooden fasteners: a critical analysis of evaluation methods and standards. Eur J Wood Prod 2025; 83: 143. https://doi.org/10.1007/s00107-025-02293-1.

[7] Li H, Feng Z, Shen X, Wang Y, Xue X, Lorenzo R, et al. Engineered bamboo bridge structure - Report on 3rd International Collaboration on Bamboo Construction. Sustain Struct 2024; 4. https://doi.org/10.54113/j.sust.2024.000062.

[8] Nkeuwa WN, Zhang J, Semple KE, Chen M, Xia Y, Dai C. Bamboo-based composites: A review on fundamentals and processes of bamboo bonding. Composites Part B: Engineering 2022; 235: 109776. https://doi.org/10.1016/j.compositesb.2022.109776.

[9] Fan YL, Li T, Yi JX, Xiao Y. Axial compression behaviour of bamboo-wood composite columns fabricated with glubam and laminated veneer lumber. Engineering Structures 2024; 316: 118526. https://doi.org/10.1016/j.engstruct.2024.118526.

[10] Nie Y, Wei Y, Huang L, Liu Y, Dong F. Influence of slenderness ratio and sectional geometry on the axial compression behavior of original bamboo columns. Journal of Wood Science 2021; 67: 36. https://doi.org/10.1186/s10086-021-01968-6.

[11] Yu WK, Chung KF, Chan SL. Column buckling of structural bamboo. Engineering Structures 2003; 25: 755–68. https://doi.org/10.1016/S0141-0296(02)00219-5.

[12] Verma CS, Chariar VM. Development of layered laminate bamboo composite and their mechanical properties. Composites Part B: Engineering 2012; 43: 1063–9. https://doi.org/10.1016/j.compositesb.2011.11.065.

[13] Yeh M-C, Lin Y-L. Finger joint performance of structural laminated bamboo member. J Wood Sci 2012; 58: 120–7. https://doi.org/10.1007/s10086-011-1233-7.

[14] Zhao P, Zhang X. Size effect of section on ultimate compressive strength parallel to grain of structural bamboo scrimber. Construction and Building Materials 2019; 200: 586–90. https://doi.org/10.1016/j.conbuildmat.2018.12.088.

[15] Goonewardena J, Subhani M, Reiner J, Kafle B, Ashraf M. Behaviour of short and long columns made from bamboo scrimber subjected to uniaxial compression. Advances in Bamboo Science 2024; 7: 100082. https://doi.org/10.1016/j.bamboo.2024.100082.
[16] Chen S, Wei Y, Hu Y, Zhai Z, Wang L. Behavior and strength of rectangular bamboo scrimber columns with shape and slenderness effects. Materials Today Communications 2020; 25: 101392. https://doi.org/10.1016/j.mtcomm.2020.101392.
[17] Xiao Y. Research development of glued laminated bamboo (glubam) and cross-laminated bamboo and timber (CLBT). Academic Journal of Civil Engineering, vol. 37, Belfast, UK: Academic Journal of Civil Engineering 2019; p: 658-663. https://doi.org/10.26168/ICBBM2019.95.
[18] Tan C, Li H, Wei D, Lorenzo R, Yuan C. Mechanical performance of parallel bamboo strand lumber columns under axial compression: Experimental and numerical investigation. Construction and Building Materials 2020; 231.
[19] Dong W, Wang Z, Zhou J, Gong M. Experimental study on bending properties of cross-laminated timber-bamboo composites. Construction and Building Materials 2021; 300: 124313. https://doi.org/10.1016/j.conbuildmat.2021.124313.
[20] EN 1995-1-1. Eurocode 5: Design of timber structures - Part 1-1: General - Common rules and rules for buildings. CEN, Brussels, European Standard 2008.
[21] NDS. National Design Specification (NDS) for Wood Construction. Leesburg, VA United States, American Wood Council 2018.
[22] GB 50005. Standard for design of timber structures 2017.
[23] Chen S, Wei Y, Wang G, Zhao K, Ding M. Mechanical behavior of laminated bamboo–timber composite columns under axial compression. ArchivCivMechEng 2023; 23: 72. https://doi.org/10.1007/s43452-023-00612-y.
[24] Wang Y, Huang Q, Dong H, Wang Z, Shu B, Gong M. Mechanical behavior of cross-laminated timber-bamboo short columns with different layup configurations under axial compression. Construction and Building Materials 2024; 421: 135695. https://doi.org/10.1016/j.conbuildmat.2024.135695.
[25] College of Civil Engineering, Nanjing Forestry University, Nanjing 210037, China., Li H, Xue X, College of Civil Engineering, Nanjing Forestry University, Nanjing 210037, China., Xiong Z, Ganzhou Sentai Bamboo Company LTD, Ganzhou 341001, China., et al. Application case of laminated bamboo lumber structure – Building of Sentai Bamboo Research Center. Sustain Struct 2024; 4. https://doi.org/10.54113/j. sust.2024.000043.
[26] Villegas L, Morán R, García JJ. Combined culm-slat Guadua bamboo trusses. Engineering Structures 2019; 184: 495–504. https://doi.org/10.1016/j.engstruct.2019.01.114.
[27] Wang C, Chen G, Zhang E, Zhu W, Chen F. Experimental studies on laminated bamboo trusses connected with nailed glubam plates. Structures 2025; 78: 109330. https://doi.org/10.1016/j.istruc.2025.109330.
[28] Shi D, Marano GC, Demartino C. Modeling of glubam roof truss, parameter identification and updating based on parallel genetic algorithm. Engineering Structures 2024; 316: 118520. https://doi.org/10.1016/j.engstruct.2024.118520.
[29] Ma R, Wang X, Du Y, Sun G, Kang S-B, Ma J, et al. Experimental and theoretical investigation into flexural performance of thin-walled steel-laminated bamboo lumber truss beam. Thin-Walled Structures 2024; 199: 111841. https://doi.org/10.1016/j.tws.2024.111841.
[30] Wang R, Pan HY, Li Z, Xiao Y. Mechanical Behavior of Glued Laminated Bamboo Moment-Resisting Connections. J Struct Eng 2023; 149: 04022220. https://doi.org/10.1061/JSENDH.STENG-11623.
[31] Mashrah WAH, Boufendassa R, Fu X, Al-Mansour A, Yu Y, Amer M, et al. Comprehensive review of engineered bamboo in structural engineering: Comparative insights into laminated bamboo and bamboo scrimber. Structures 2025; 76: 108896. https://doi.org/10.1016/j.istruc.2025.108896.
[32] Laemlaksakul V. Investigation of performance of laminated bamboo chair through virtual testing. 10th WSEAS international conference on Mathematical and computational methods in science and engineering, Bucharest Romania: WSEAS; 2008: 44. https://dl.acm.org/doi/proceedings/10.5555/1569549.
[33] Li H, Xue X, Xiong Z, Ashraf M, Lorenzo R, Shuchi S. Application case of laminated bamboo lumber structure – Building of Sentai Bamboo Research Center. Sustain Struct 2024; 4. https://doi.org/10.54113/j.sust.2024.000043.
[34] ISO 23478. Bamboo structures — Engineered bamboo products — Test methods for determination of physical and mechanical properties 2022.
[35] ASTM D198. Standard Test Methods of Static Tests of Lumber in Structural Sizes 2022. https://doi.org/10.1520/D0198-22a.
[36] Yang D, Li H, Xiong Z, Mimendi L, Lorenzo R, Corbi I, et al. Mechanical properties of laminated bamboo under off-axis compression. Composites Part A: Applied Science and Manufacturing 2020; 138: 106042. https://doi.org/10.1016/j.compositesa.2020.106042.
[37] Subhani M, Lui HY. Effect of Primer and Fibre Orientation on Softwood–Hardwood Bonding. Journal of

Composites Science 2024; 8: 192. https://doi.org/10.3390/jcs8060192.
[38] Wei Y, Zhou M, Zhao K, Zhao K, Li G. Stress–strain relationship model of glulam bamboo under axial loading. Advanced Composites Letters 2020; 29: 2633366X20958726. https://doi.org/10.1177/2633366X20958726.
[39] Popovics S. A numerical approach to the complete stress-strain curve of concrete. Cement and Concrete Research 1973; 3: 583–99. https://doi.org/10.1016/0008-8846(73)90096-3.
[40] Sargin M. Stress-strain relationships for concrete and the analysis of structural concrete sections. Waterloo, Ont: University of Waterloo; 1971.
[41] Richard RM, Abbott BJ. Versatile Elastic-Plastic Stress-Strain Formula. Journal of the Engineering Mechanics Division 1975; 101: 511–5. https://doi.org/10.1061/JMCEA3.0002047.
[42] ABARES. Australia's forests at a glance 2019 with data to 2017–18. Canberra: ABARES 2019.
[43] AS 1720.1. Timber structures Part 1: Design methods 2010.
[44] Forest Products Laboratory. Wood handbook: Wood as an engineering material. Madison, WI: U.S. Department of Agriculture, Forest Service, Forest Products Laboratory 2021.